

Attochemical Control of Nuclear Motion Despite Fast Electronic Decoherence

Lina Fransén,[†] Sandra Gómez,[‡] and Morgane Vacher^{*,†}

[†]*Nantes Université, CNRS, CEISAM UMR 6230, F-44000 Nantes, France*

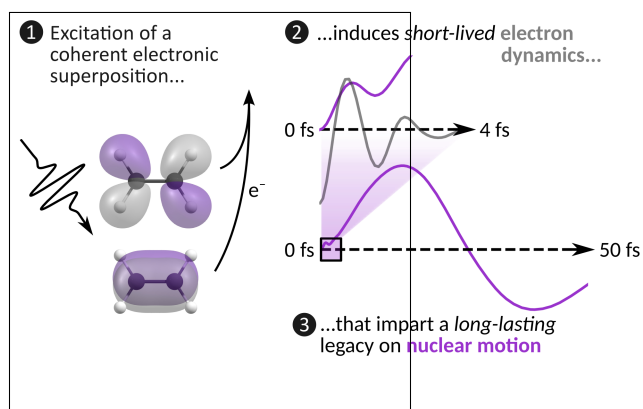
[‡]*Department of Chemistry, Universidad Autónoma de Madrid, C. Francisco Tomás y
Valiente, 7, 28049 Madrid*

E-mail: morgane.vacher@univ-nantes.fr

Abstract

Short-in-time, broad-in-energy atto- or few-femtosecond pulses can excite coherent superpositions of several electronic states in molecules. This results in ultrafast charge oscillations known as charge migration. A key open question in the emerging field of attochemistry is whether these electron dynamics, which due to decoherence often last only for a few femtoseconds, can influence longer-timescale nuclear rearrangements. Herein, we address this question through full-dimensional quantum dynamics simulations of the coupled electron-nuclear dynamics initiated by ionization and coherent excitation of ethylene. The simulations on this prototype organic chromophore predict electronic coherences with half-lives of less than one femtosecond. Despite their brevity, these electronic coherences induce vibrational coherences along the derivative coupling vectors that persist for at least 50 fs. These results suggest that short-lived electronic coherences can impart long-lasting legacies on nuclear motion, a finding of potential importance to the interpretation of attosecond experiments and the development of strategies for attochemical control.

TOC Graphic



The experimental realization of attosecond pulses at the beginning of the 21st century^{1,2} has enabled the excitation of coherent superpositions of electronic states in photoionized molecules. This results in a purely electronic motion, known as charge migration,³ where the hole density oscillates along the molecular backbone with frequencies defined by the energy gaps between the involved electronic states. Control of the motion of the electrons—the particles responsible for chemical bonds—through the excitation of tailored electronic wave packets may open up the possibility of steering chemical reactivity toward a desired outcome. This is the paradigm of attochemistry,^{4–6} which offers an alternative to femtochemical control strategies^{7–12} that seek to steer reactivity by instead controlling the nuclear motion through the excitation of tailored nuclear wave packets. However, electronic coherences in molecules often only last for a few femtoseconds.^{13–18} This is widely believed to pose a challenge for controlling chemical transformations attochemically,^{5,18–21} as these unfold on much longer timescales.

This letter demonstrates theoretically that short-lived electronic coherences can impart long-lasting legacies on the nuclear motion. This is done through quantum dynamics simulations of ethylene upon ionization to its three lowest-lying cationic electronic states (\tilde{X} , \tilde{A} , and \tilde{B}). Ethylene cation is the simplest organic π radical and has previously been extensively studied experimentally using attosecond technology^{22–27} and theoretically through non-adiabatic dynamics simulations.^{23,24,27–31}

As an illustrative case, we focus on in-phase coherent superpositions of pairs of equally weighted cationic diabatic electronic states. The conclusions are, however, expected to be generalizable to other superpositions; this is supported by results for three-state superpositions (Section S8 of the Supporting Information). The initial wavefunctions read

$$\begin{aligned}\Psi(\mathbf{r}, \mathbf{Q}, t = 0) &= [c_i \psi_i(\mathbf{r}) + c_j \psi_j(\mathbf{r}) e^{i\varphi}] \chi_0(\mathbf{Q}, t = 0) \\ &= \Psi_{\text{el}}(\mathbf{r}) \chi_0(\mathbf{Q}, t = 0)\end{aligned}\tag{1}$$

where $c_i = c_j = 1/\sqrt{2}$ are the coefficients of the diabatic electronic states ψ_i and ψ_j , $\varphi = 0$ is the initial relative phase between the electronic states, and χ_0 is the ground state vibrational wave function of neutral ethylene. Two superpositions are considered: one comprising the \tilde{X} and \tilde{A} states, and another involving the \tilde{A} and \tilde{B} states. Figure 1 displays the hole (i.e., singly occupied) orbitals that characterize the individual \tilde{X} , \tilde{A} , and \tilde{B} states, along with schematic representations of the holes created upon ionization and excitations of the $\tilde{X}+\tilde{A}$ and $\tilde{A}+\tilde{B}$ coherent superpositions. Due to interference, the hole densities of the coherent superpositions are time-dependent and differ from the incoherent averages of the hole densities of the individual states.

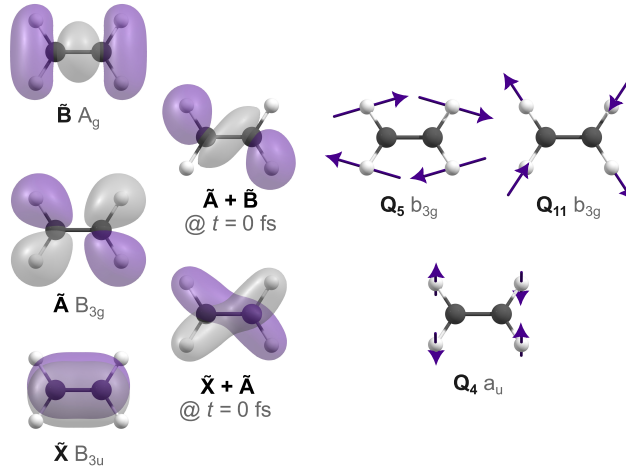


Figure 1: Left: Isodensity plots of the hole (i.e., singly occupied) molecular orbitals that characterize the individual \tilde{X} , \tilde{A} , and \tilde{B} states. Middle: Schematic representation of the holes associated with the $\tilde{X}+\tilde{A}$ and $\tilde{A}+\tilde{B}$ coherent superpositions. Right: The vibrational normal modes along which the inter-state gradients (defined in Equation 7) are non-zero for the two coherent superpositions.

Here, we note in passing that one-photon ionization to the $\tilde{X} + \tilde{A}$ superposition would, within the electric dipole approximation, result in a fully incoherent state, as the hole orbitals—and thus the photoelectrons—associated with the \tilde{X} and \tilde{A} channels have opposite parities. A coherent superposition of the \tilde{X} and \tilde{A} states may, nevertheless, be realizable using a sequence of pulses (cf. Ref. 32, where a coherent superposition of the Σ_g^+ and Σ_u^+ states of D_2^+ was generated experimentally).

A fully quantum mechanical treatment of the coupled electron-nuclear dynamics is required to adequately simulate the nuclear motion induced by coherent superpositions of electronic states.³³ Here, we employ one of the most accurate approaches—the multilayer multiconfiguration time-dependent Hartree (ML-MCTDH)³⁴ method—combined with a vibronic coupling Hamiltonian³⁵ parametrized along the 12 vibrational normal modes of ethylene. The simulations are performed in full nuclear dimensionality to adequately capture the electronic decoherence: previous work has shown that decoherence can result from the interplay of many vibrational modes.¹⁶

Vibronic coupling models have previously been used to calculate photoelectron spectra of ethylene.^{36–39} In the present work, the vibronic coupling Hamiltonian, which is diabatic by ansatz, reads

$$\mathbf{H} = \left(\hat{T}_{\text{N}} + V_0 \right) \mathbf{1} + \mathbf{W} \quad (2)$$

where \hat{T}_{N} is the nuclear kinetic energy operator, V_0 is the zero-order diabatic potential, and \mathbf{W} is the diabatic potential energy matrix. The latter is expanded in a Taylor series around the equilibrium geometry of neutral ethylene in the basis of mass-frequency scaled normal mode coordinates. Its on- and off-diagonal elements read

$$W_{ii}(\mathbf{Q}) = E_i + \sum_{\alpha}^f \kappa_{\alpha}^{(i)} Q_{\alpha} + \sum_{\alpha}^f \frac{1}{2} \gamma_{\alpha,\alpha}^{(i)} Q_{\alpha}^2 \quad (3)$$

$$W_{ij}(\mathbf{Q}) = \sum_{\alpha}^f \lambda_{\alpha}^{(i,j)} Q_{\alpha} \quad (4)$$

where E_i is the vertical ionization energy of the cationic electronic state ψ_i , $\kappa_{\alpha}^{(i)}$ and $\gamma_{\alpha,\alpha}^{(i)}$ are the linear and quadratic intra-state coupling constants on state ψ_i along normal mode Q_{α} , and $\lambda_{\alpha}^{(i,j)}$ is the linear inter-state coupling constant between states ψ_i and ψ_j along mode Q_{α} . The effect of including bilinear intra-state coupling constants ($\gamma_{\alpha,\beta}^{(i)}$, $\alpha \neq \beta$) is discussed in Section S6 of the Supporting Information. The parameters entering the model Hamiltonian

were obtained from a least-square fit to SA5-CASSCF(11e,12o) energies. Details of the active space are provided in Section S1 of the Supporting Information. The *ab initio* energies were calculated with OpenMolcas^{40–42} using the ANO-RCC-VDZP⁴³ basis set and the atomic compact Cholesky decomposition.⁴⁴ The fitting, performed with the VCHam programs in the Quantics software,⁴⁵ was facilitated by the high point group symmetry (D_{2h}) of ethylene, as the following selection rules limit the number of non-zero parameters:

$$\kappa_{\alpha}^{(i)} \neq 0 : \Gamma_{\alpha} \supset \Gamma_A \quad (5a)$$

$$\lambda_{\alpha}^{(i,j)} \neq 0 : \Gamma_{\alpha} \otimes \Gamma_i \otimes \Gamma_j \supset \Gamma_A \quad (5b)$$

where Γ_A is the totally symmetric irreducible representation of the point group, Γ_{α} is a vibrational symmetry, and Γ_i and Γ_j are electronic state symmetries. The quadratic intra-state coupling constants are symmetry-allowed for all vibrational modes on all electronic states ($\gamma_{\alpha,\alpha}^{(i)} \neq 0 : \Gamma_{\alpha} \otimes \Gamma_{\alpha} \supset \Gamma_A$). Further details on the model Hamiltonian are reported in Section S1 of the Supporting Information, and the robustness of the results with respect to the model parameters is discussed in Section S7. Details on the ML-MCTDH simulations, which were performed with Quantics,⁴⁵ using (where possible) an adaptive number of single particle functions,⁴⁶ are provided in Section S2.

The electronic population decays obtained using the model Hamiltonian in MCTDH simulations initiated on the individual \tilde{A} and \tilde{B} states are in good agreement with results from previous on-the-fly surface hopping simulations³⁰ (Section S3 of the Supporting Information). For a fair comparison, the electronic populations from the MCTDH simulations were transformed from the diabatic to the adiabatic representation.^{47,48} Moreover, the time scale of the electronic relaxation following ionization to the individual \tilde{A} state is consistent with experimental results obtained through attosecond transient absorption spectroscopy.²⁴ These

agreements with previous results provide validation for the present model Hamiltonian. We acknowledge, however, that the model Hamiltonian is limited to describing the dynamics during the first ~ 50 fs after ionization, before the onset of large-amplitude nuclear motion. This and other limitations are discussed in Section S3 of the Supporting Information.

The time evolutions of the diabatic electronic populations following excitations of the $\tilde{X}+\tilde{A}$ and $\tilde{A}+\tilde{B}$ superpositions are reported in the left-hand side of Figure 2. The results for the coherent superpositions are compared with incoherent averages of simulation results obtained upon excitations of the individual \tilde{X} , \tilde{A} , and \tilde{B} states. Quantum coherences between the initially populated states do not significantly influence the population decays, as evidenced by the close agreement between the results for the coherent superpositions and the incoherent averages.

Electronic state population transfer, dephasing due to the nuclear wave packet width, and loss of overlap between nuclear wave packets associated with different electronic states can lead to electronic decoherence.^{26,49} The degree of electronic coherence can be measured using the electronic purity, $\text{Tr}(\rho^2)$, where Tr denotes the trace and ρ is the reduced density matrix. The elements of the reduced density matrix read

$$\begin{aligned}\rho_{ij} &= \int d\mathbf{Q} \langle \psi_i(\mathbf{r}) | \Psi(\mathbf{r}, \mathbf{Q}, t) \rangle \langle \Psi(\mathbf{r}, \mathbf{Q}, t) | \psi_j(\mathbf{r}) \rangle \\ &= \int d\mathbf{Q} \chi_i(\mathbf{Q}, t) \chi_j^*(\mathbf{Q}, t)\end{aligned}\tag{6}$$

where the on-diagonal terms ρ_{ii} represent the electronic populations and the off-diagonal ones ρ_{ij} correspond to the electronic coherences. The right-hand side of Figure 2 reports the term $M_{\text{coh}} = 2\rho_{ij}\rho_{ji}$,^{26,49} which quantifies the electronic coherence by gathering the off-diagonal components of $\text{Tr}(\rho^2)$. One can show that $M_{\text{coh}} \leq 2\rho_{ii}\rho_{jj}$.²⁶ At $t = 0$ fs, $M_{\text{coh}}=0.5$, the theoretical maximum for equally weighted two-state superpositions. Decoherence then occurs rapidly, with M_{coh} dropping to half of its initial value after ~ 0.8 fs and ~ 0.7 fs for the $\tilde{X}+\tilde{A}$ and the $\tilde{A}+\tilde{B}$ superpositions, respectively. Similar decoherence time scales have previously

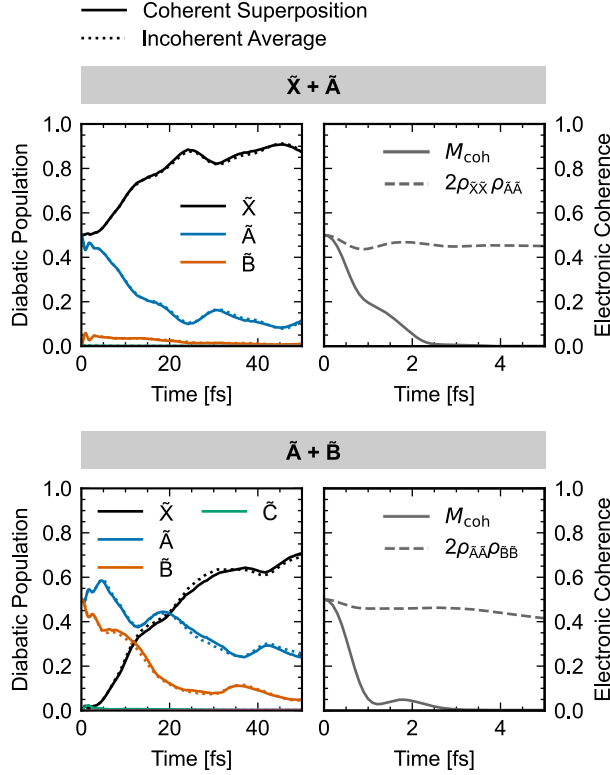


Figure 2: Left: Time evolutions of the diabatic electronic populations following excitations of the $\tilde{X} + \tilde{A}$ (top) and the $\tilde{A} + \tilde{B}$ (bottom) equally weighted in-phase coherent superpositions. The dotted lines represent the incoherent averages of the population dynamics obtained following excitations of the relevant individual electronic states. Right: Degrees of electronic coherence (solid lines) and their upper bounds based on the electronic populations (dashed lines) following excitations of the $\tilde{X} + \tilde{A}$ (top) and $\tilde{A} + \tilde{B}$ (bottom) coherent superpositions. Note that the x-axis ranges for the right-hand side plots are ten times shorter than for the left plots.

been reported in theoretical studies on other molecules.^{13–18} In the present case, the rapid electronic decoherences are not primarily due to electronic state population transfers, as the M_{coh} values decay much more quickly than the $2\rho_{ii}\rho_{jj}$ values. Instead, the decoherence is mainly caused by dephasing due to the nuclear wave packet width and loss of overlap between nuclear wave packets associated with different electronic states. Given the rapidity of the decoherence, it is reasonable to assume that the former mechanism—dephasing—dominates. Unlike the latter, this mechanism does not require nuclear wave packets to move; it can occur due to the width of the nuclear wave packets instantaneously after ionization. Dephasing has been identified as the main cause of decoherence in previous fully quantum mechanical

dynamics studies on other molecules.^{13,16}

Having established that the electronic coherences are short-lived and do not affect the electronic population decays, we now investigate their impact on the nuclear motion. The nuclear energy gradient at $Q = 0$ and $t = 0$ fs along normal mode Q_α for a coherent superposition described by Equation 1 is given by⁵⁰

$$\begin{aligned} \frac{\partial}{\partial Q_\alpha} \langle \Psi_{\text{el}}(\mathbf{r}) | \hat{H}_{\text{el}} | \Psi_{\text{el}}(\mathbf{r}) \rangle &= |c_i|^2 \kappa_\alpha^{(i)} \\ &+ |c_j|^2 \kappa_\alpha^{(j)} + 2|c_i||c_j|\cos(\varphi)\lambda_\alpha^{(i,j)} \end{aligned} \quad (7)$$

where \hat{H}_{el} is the potential part of the Hamiltonian defined in Equation 2. We note that Equation 7 holds for all normal modes except for Q_{10} , for which V_0 has a non-zero gradient at $Q = 0$ (Section S1 of the Supporting Information). The first two terms on the right-hand side of Equation 7 represent the gradients of the individual electronic states, referred to as the intra-state gradients, weighted by the state populations. The last term, which is directed along the derivative coupling vector and termed the inter-state gradient, stems from interference between the wave packet components on the two electronic states. This last term is thus the “attochemical” component of the gradient, and the following discussion focuses on the nuclear motion that it induces. The symmetry selection rule for $\lambda_\alpha^{(i,j)}$ in Equation 5b dictates that the inter-state gradient is directed along the torsional mode Q_4 for the $\tilde{X}+\tilde{A}$ coherent superposition, and has components along modes Q_5 and Q_{11} for the $\tilde{A}+\tilde{B}$ superposition. The displacement vectors for the three modes are shown in Figure 1.

The time evolutions of the nuclear densities along Q_4 following excitation of the $\tilde{X}+\tilde{A}$ coherent superposition, and along Q_5 and Q_{11} following excitation of the $\tilde{A}+\tilde{B}$ superposition, are shown in the top panels of Figure 3. The nuclear densities evolve asymmetrically along these normal modes, as highlighted by the plots of $Q_\alpha(q) - Q_\alpha(-q)$. By the symmetry selection rule for $\kappa_\alpha^{(i)}$ in Equation 5a, the intra-state gradients are zero along Q_4 , Q_5 , and Q_{11} , suggesting that the inter-state gradients are responsible for this behavior. This is

confirmed by the absence of asymmetry for the incoherent averages presented in the bottom panels of Figure 3. Notably, the nuclear density asymmetries, which thus stem from the coherences between the initially populated electronic states, persist throughout the 50 fs simulation time—despite the much faster timescale of electronic decoherence.

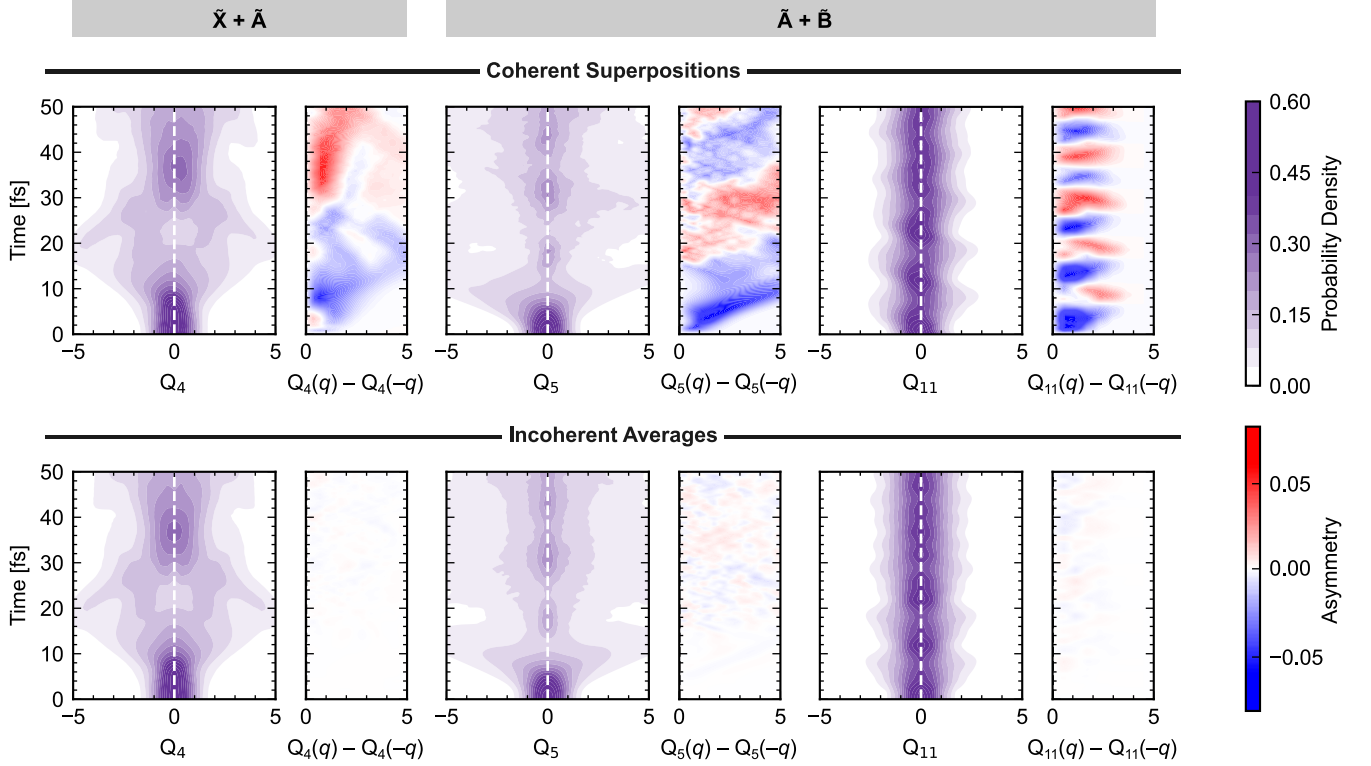


Figure 3: Top: Time evolutions of reduced nuclear densities and nuclear density asymmetries following excitations of the $\tilde{X} + \tilde{A}$ (left) and the $\tilde{A} + \tilde{B}$ (right) equally weighted in-phase coherent superpositions. The results are shown along the normal modes that exhibit non-zero inter-state gradients for each superposition. Bottom: Same as the top panel, but for the incoherent averages of the dynamics observed following excitations to the relevant individual electronic states.

The nuclear density asymmetries in Figure 3 exhibit sinusoidal temporal modulations. To investigate the nature of this oscillatory behaviour, Figure 4 reports the position expectation values along Q_4 , Q_5 and Q_{11} . We address first the early-time nuclear dynamics that take place before electronic decoherence. These are shown in the insets of Figure 4. The insets also display the electron dynamics, represented by the sum of the off-diagonal elements of the reduced density matrix ($\rho_{ij} + \rho_{ji}$). The electron dynamics oscillate between 1 and -1 as

the hole migrates across the molecular backbone. The oscillations are damped rapidly due to decoherence. The periods of the oscillations align well with those predicted from the energy gaps between the electronic state pairs at the Franck-Condon point: $\hbar/(E_{\tilde{A}} - E_{\tilde{X}}) = 1.45$ fs and $\hbar/(E_{\tilde{B}} - E_{\tilde{A}}) = 2.54$ fs for the $\tilde{X}+\tilde{A}$ and $\tilde{A}+\tilde{B}$ superpositions, respectively.

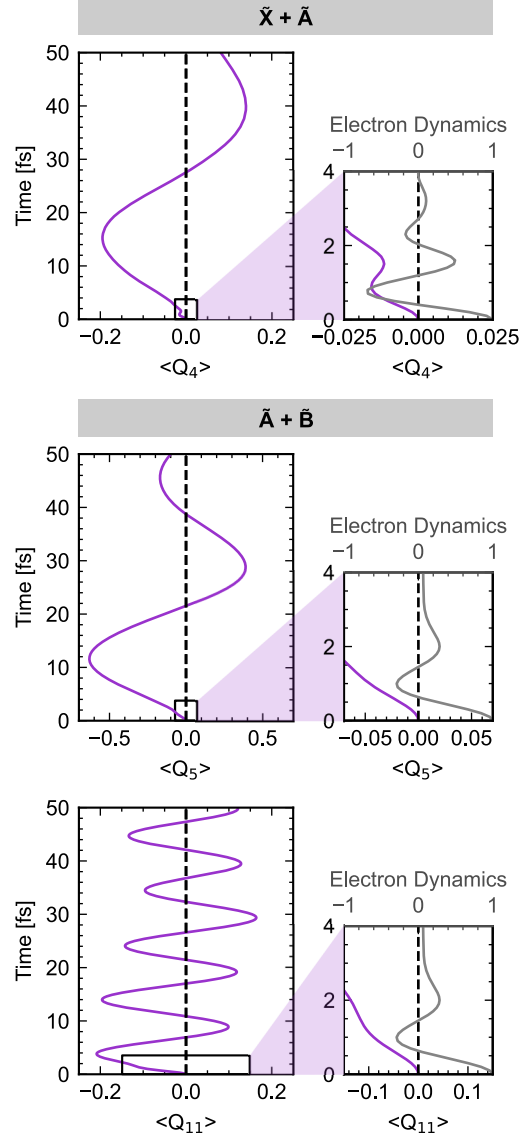


Figure 4: Time evolutions of nuclear position expectation values following excitations of the $\tilde{X}+\tilde{A}$ (top) and $\tilde{A}+\tilde{B}$ (bottom) equally weighted in-phase coherent superpositions. The results are shown along the normal modes that exhibit non-zero inter-state gradients for each superposition. The insets show magnifications of the early-time position expectation values, along with the electron dynamics, defined as $\rho_{ij} + \rho_{ji}$. Note that the x-axis ranges differ between the normal modes.

The electron dynamics produce instantaneous inter-state nuclear gradients, leading to small-amplitude oscillations in the nuclear position expectation values at the same frequencies. This effect is most clearly seen for the $\tilde{X}+\tilde{A}$ superposition. The signs of these oscillations can be reversed in a predictable (Equation 7) and well-documented^{14,26,50} fashion by changing the relative phase between the electronic states comprising the superpositions from $\varphi=0$ to π (Section S4 of the Supporting Information).

The small-amplitude, short-period oscillations in the position expectation values observed before electronic decoherence are superimposed on larger-amplitude, slower oscillations that persist throughout the simulations (main panels of Figure 4). Damped oscillations in a nuclear coordinate, driven by electron dynamics, overlaid on a slower evolution, have previously been reported in on-the-fly Ehrenfest simulations of modified bismethylene-adamantane,²⁶ though the nature and lifetime of the slow evolution were not addressed in that study. More broadly, to our knowledge, the impact of initial electronic coherences in a polyatomic molecule on the nuclear dynamics *after* decoherence has not been addressed theoretically in the literature. Upon excitation of the $\tilde{A}+\tilde{B}$ superposition, the periods of the slow oscillations that persist beyond electronic decoherence differ along Q_5 and Q_{11} , suggesting that they are characteristic of the vibrational normal modes rather than of the electron dynamics. Indeed, the periods observed in the main panels in Figure 4 agree well with those of the respective vibrational normal modes (Section S5 of the Supporting Information). As is the case for the small-amplitude, short-period oscillations driven by the electron dynamics, the signs of the larger-amplitude oscillations with frequencies characteristic of the vibrational normal modes can be reversed by changing the relative phase between the electronic states at $t = 0$ fs from $\varphi = 0$ to π (Section S4 of the Supporting Information). This, together with the absence of oscillations for the incoherent averages (bottom panels in Figure 3, and Figures S10 and S11 of the Supporting Information), demonstrates that the long-lived nuclear oscillations stem from the short-lived coherences between the initially populated electronic states.

The theoretical findings reported herein share similarities with recent experimental results

reported by Schwickert et al. and their associated interpretation.^{51,52} In their work, a coupling of electronic to vibronic coherences was proposed to explain sinusoidal temporal modulations with shifting periods in time-resolved spectra of glycine cation.

To conclude, the simulations presented in this letter predict that short-lived electronic coherences can induce vibrational coherences with significantly longer lifetimes. For ethylene cation, considered herein as a prototype case, the vibrational coherences persist throughout the 50 fs simulation time. Beyond this time frame, ethylene cation dissociates via H- and H₂-loss.³⁰ The next step is to investigate whether the yields of these dissociation channels can be controlled through rationally designed coherent superpositions. Such control of bond breaking represents the true goal of att chemistry. Theoretically, addressing this challenge would require either the development of a more sophisticated model Hamiltonian capable of describing large-amplitude nuclear motions or the use of an on-the-fly quantum dynamics method such as DD-vMCG.⁵³ We stress, however, that whether short-lived electronic coherences can leave sufficiently large imprints on the nuclear motion to affect the chemical outcome remains an open question. An interesting direction for future research could be to systematically investigate how to maximize the amplitude of this imprint. We hypothesize that, in addition to ensuring roughly equal weights of the coherently populated states and strong inter-state couplings close to the Franck-Condon point (see Equation 7), the relative duration of the coherence compared to the period of the electron dynamics may be a key factor. Specifically, it may be ideal if the electron dynamics are damped by decoherence before they reverse direction. Moreover, a relatively long electron dynamics period (i.e., a small energy gap at the Franck-Condon point) may be advantageous, as this allows the force on the nuclei to act in a single direction for a longer time.

Acknowledgement

This work received financial support under the EUR LUMOMAT project and the Investments for the Future program ANR-18-EURE-0012 (M.V. and L.F.) L.F. acknowledges thesis funding from the Région Pays de la Loire and Nantes University. The project is also partly funded by the European Union through ERC Grant No. 101040356 (M. V.). The views and opinions expressed are however those of the authors only and do not necessarily reflect those of the European Union or the European Research Council Executive Agency. Neither the European Union nor the granting authority can be held responsible for them. S.G. also thanks the EPSRC under the COSMOS programme grant (EP/X026973/1). The simulations in this work were performed using HPC resources from CCIPL (Le centre de calcul intensif des Pays de la Loire) and from GENCI-IDRIS (Grant 2021-101353).

Supporting Information Available

Details on the vibronic coupling model Hamiltonian, computational details for (ML-)MCTDH simulations, validation and limitations of the model Hamiltonian, position expectation values along all normal modes for in-phase and out-of-phase superpositions, rationalization of the frequencies of the nuclear motion asymmetries, effect of including bilinear on-diagonal coupling constants, sensitivity to the inter-state coupling strength, computational details and results for three-state superpositions.

References

- (1) Paul, P. M.; Toma, E. S.; Breger, P.; Mullot, G.; Augé, F.; Balcou, P.; Muller, H. G.; Agostini, P. Observation of a Train of Attosecond Pulses from High Harmonic Generation. *Science* **2001**, *292*, 1689–1692.
- (2) Hentschel, M.; Kienberger, R.; Spielmann, C.; Reider, G. A.; Milosevic, N.; Brabec, T.;

- Corkum, P.; Heinzmann, U.; Drescher, M.; Krausz, F. Attosecond metrology. *Nature* **2001**, *414*, 509–513.
- (3) Cederbaum, L.; Zobeley, J. Ultrafast charge migration by electron correlation. *Chemical Physics Letters* **1999**, *307*, 205–210.
- (4) Lépine, F.; Ivanov, M. Y.; Vrakking, M. J. J. Attosecond molecular dynamics: fact or fiction? *Nature Photonics* **2014**, *8*, 195–204.
- (5) Merritt, I. C. D.; Jacquemin, D.; Vacher, M. Attochemistry: Is Controlling Electrons the Future of Photochemistry? *The Journal of Physical Chemistry Letters* **2021**, *12*, 8404–8415.
- (6) Calegari, F.; Martin, F. Open questions in attochemistry. *Communications Chemistry* **2023**, *6*, 184.
- (7) Shapiro, M.; Brumer, P. On the Origin of Pulse Shaping Control of Molecular Dynamics. *The Journal of Physical Chemistry A* **2001**, *105*, 2897–2902.
- (8) Brumer, P.; Shapiro, M. One photon mode selective control of reactions by rapid or shaped laser pulses: An emperor without clothes? *Chemical Physics* **1989**, *139*, 221–228.
- (9) Charron, E.; Giusti-Suzor, A.; Meis, F. H. Coherent control of photodissociation in intense laser fields. *The Journal of Chemical Physics* **1995**, *103*, 7359–7373.
- (10) Tannor, D. J.; Kosloff, R.; Rice, S. A. Coherent pulse sequence induced control of selectivity of reactions: Exact quantum mechanical calculations. *The Journal of Chemical Physics* **1986**, *85*, 5805–5820.
- (11) Assion, A.; Baumert, T.; Bergt, M.; Brixner, T.; Kiefer, B.; Seyfried, V.; Strehle, M.; Gerber, G. Control of Chemical Reactions by Feedback-Optimized Phase-Shaped Femtosecond Laser Pulses. *Science* **1998**, *282*, 919–922.

- (12) Brixner, T.; Damrauer, N. H.; Niklaus, P.; Gerber, G. Photoselective adaptive femtosecond quantum control in the liquid phase. *Nature* **2001**, *414*, 57–60.
- (13) Vacher, M.; Bearpark, M. J.; Robb, M. A.; Malhado, J. P. Electron Dynamics upon Ionization of Polyatomic Molecules: Coupling to Quantum Nuclear Motion and Decoherence. *Physical Review Letters* **2017**, *118*, 083001.
- (14) Arnold, C.; Vendrell, O.; Welsch, R.; Santra, R. Control of Nuclear Dynamics through Conical Intersections and Electronic Coherences. *Physical Review Letters* **2018**, *120*, 123001.
- (15) Scheidegger, A.; Vaníček, J.; Golubev, N. V. Search for long-lasting electronic coherence using on-the-fly ab initio semiclassical dynamics. *The Journal of Chemical Physics* **2022**, *156*, 034104.
- (16) Arnold, C.; Vendrell, O.; Santra, R. Electronic decoherence following photoionization: Full quantum-dynamical treatment of the influence of nuclear motion. *Physical Review A* **2017**, *95*, 033425.
- (17) Jia, D.; Manz, J.; Yang, Y. De- and Recoherence of Charge Migration in Ionized Iodoacetylene. *The Journal of Physical Chemistry Letters* **2019**, *10*, 4273–4277.
- (18) Despré, V.; Golubev, N. V.; Kuleff, A. I. Charge Migration in Propiolic Acid: A Full Quantum Dynamical Study. *Physical Review Letters* **2018**, *121*, 203002.
- (19) Nisoli, M. Attosecond science the art of making electron movies. *Europhysics News* **2024**, *55*, 22–25.
- (20) Vester, J.; Despré, V.; Kuleff, A. I. The role of symmetric vibrational modes in the decoherence of correlation-driven charge migration. *The Journal of Chemical Physics* **2023**, *158*, 104305.

- (21) Alexander, O. G.; Marangos, J. P.; Ruberti, M.; Vacher, M. In *Advances in Atomic, Molecular, and Optical Physics*; DiMauro, L. F., Perrin, H., Yelin, S. F., Eds.; Advances In Atomic, Molecular, and Optical Physics; Academic Press, 2023; Vol. 72; pp 183–251.
- (22) van Tilborg, J.; Allison, T. K.; Wright, T. W.; Hertlein, M. P.; Falcone, R. W.; Liu, Y.; Merdji, H.; Belkacem, A. Femtosecond Isomerization Dynamics in the Ethylene Cation Measured in an EUV-pump NIR-probe Configuration. *Journal of Physics B: Atomic, Molecular and Optical Physics* **2009**, *42*, 081002.
- (23) Ludwig, A.; Liberatore, E.; Herrmann, J.; Kasmi, L.; López-Tarifa, P.; Gallmann, L.; Rothlisberger, U.; Keller, U.; Lucchini, M. Ultrafast Relaxation Dynamics of the Ethylene Cation C_2H_4^+ . *The Journal of Physical Chemistry Letters* **2016**, *7*, 1901–1906.
- (24) Zinchenko, K. S.; Ardana-Lamas, F.; Seidu, I.; Neville, S. P.; van der Veen, J.; Lanfaloni, V. U.; Schuurman, M. S.; Wörner, H. J. Sub-7-Femtosecond Conical-Intersection Dynamics Probed at the Carbon K-edge. *Science* **2021**, *371*, 489–494.
- (25) Lucchini, M.; Mignolet, B.; Murari, M.; Gonçalves, C. E. M.; Lucarelli, G. D.; Frassetto, F.; Poletto, L.; Remacle, F.; Nisoli, M. Few-Femtosecond C_2H_4^+ Internal Relaxation Dynamics Accessed by Selective Excitation. *The Journal of Physical Chemistry Letters* **2022**, *13*, 11169–11175.
- (26) Vacher, M.; Albertani, F. E. A.; Jenkins, A. J.; Polyak, I.; Bearpark, M. J.; Robb, M. A. Electron and nuclear dynamics following ionisation of modified bismethylene-adamantane. *Faraday Discussions* **2016**, *194*, 95–115.
- (27) Lucchini, M.; Cardoso-Gutierrez, M.; Murari, M.; Frassetto, F.; Poletto, L.; Nisoli, M.; Remacle, F. Isotope Effect on the Few-Femtosecond Relaxation Dynamics of the Ethylene Cation. *The Journal of Physical Chemistry A* **2025**, *129*, 3063–3070.
- (28) Joalland, B.; Mori, T.; Martínez, T. J.; Suits, A. G. Photochemical Dynamics of Ethylene Cation C_2H_4^+ . *The Journal of Physical Chemistry Letters* **2014**, *5*, 1467–1471.

- (29) Vacher, M.; Boyer, A.; Lorient, V.; Lépine, F.; Nandi, S. Few-Femtosecond Isotope Effect in Polyatomic Molecules Ionized by Extreme Ultraviolet Attosecond Pulse Trains. *The Journal of Physical Chemistry A* **2022**, *126*, 5692–5701.
- (30) Fransén, L.; Tran, T.; Nandi, S.; Vacher, M. Dissociation and Isomerization Following Ionization of Ethylene: Insights from Nonadiabatic Dynamics Simulations. *The Journal of Physical Chemistry A* **2024**, *128*, 1457–1465.
- (31) Tran, T.; Worth, G. A.; Robb, M. A. Coherent Excitation of the CH Stretching Vibrations in C_2H_4^+ The Role of the Derivative Coupling Studied by the Quantum Ehrenfest Method. *Journal of Computational Chemistry* **2025**, *46*, e70028.
- (32) Sansone, G.; Kelkensberg, F.; Pérez-Torres, J. F.; Morales, F.; Kling, M. F.; Siu, W.; Ghafur, O.; Johnsson, P.; Swoboda, M.; Benedetti, E. et al. Electron localization following attosecond molecular photoionization. *Nature* **2010**, *465*, 763–766.
- (33) Tran, T.; Ferté, A.; Vacher, M. Simulating Attochemistry: Which Dynamics Method to Use? *The Journal of Physical Chemistry Letters* **2024**, *15*, 3646–3652.
- (34) Wang, H.; Thoss, M. Multilayer formulation of the multiconfiguration time-dependent Hartree theory. *The Journal of Chemical Physics* **2003**, *119*, 1289–1299.
- (35) Köppel, H.; Domcke, W.; Cederbaum, L. S. In *Advances in Chemical Physics*; Prigogine, I., Rice, S. A., Eds.; John Wiley & Sons, Ltd, 1984; pp 59–246.
- (36) Köppel, H.; Domcke, W.; Cederbaum, L. S.; Niessen, W. v. Vibronic coupling effects in the photoelectron spectrum of ethylene. *The Journal of Chemical Physics* **1978**, *69*, 4252–4263.
- (37) Köppel, H.; Cederbaum, L. S.; Domcke, W. Strong nonadiabatic effects and conical intersections in molecular spectroscopy and unimolecular decay: C_2H_4^+ . *The Journal of Chemical Physics* **1982**, *77*, 2014–2022.

- (38) Hazra, A.; Nooijen, M. Vibronic coupling in the excited cationic states of ethylene: Simulation of the photoelectron spectrum between 12 and 18eV. *The Journal of Chemical Physics* **2005**, *122*, 204327.
- (39) Hazra, A.; Nooijen, M. Comparison of various Franck–Condon and vibronic coupling approaches for simulating electronic spectra: The case of the lowest photoelectron band of ethylene. *Phys. Chem. Chem. Phys.* **2005**, *7*, 1759–1771.
- (40) Fdez. Galván, I.; Vacher, M.; Alavi, A.; Angeli, C.; Aquilante, F.; Autschbach, J.; Bao, J. J.; Bokarev, S. I.; Bogdanov, N. A.; Carlson, R. K. et al. OpenMolcas: From Source Code to Insight. *Journal of Chemical Theory and Computation* **2019**, *15*, 5925–5964.
- (41) Li Manni, G.; Fdez. Galván, I.; Alavi, A.; Aleotti, F.; Aquilante, F.; Autschbach, J.; Avagliano, D.; Baiardi, A.; Bao, J. J.; Battaglia, S. et al. The OpenMolcas Web: A Community-Driven Approach to Advancing Computational Chemistry. *Journal of Chemical Theory and Computation* **2023**, *19*, 6933–6991.
- (42) OpenMolcas v22.10. <https://gitlab.com/Molcas/OpenMolcas/-/releases/v22.10>, (Accessed October 2022).
- (43) Roos, B. O.; Lindh, R.; Malmqvist, P.-Å.; Veryazov, V.; Widmark, P.-O. Main Group Atoms and Dimers Studied with a New Relativistic ANO Basis Set. *The Journal of Physical Chemistry A* **2004**, *108*, 2851–2858.
- (44) Aquilante, F.; Gagliardi, L.; Pedersen, T. B.; Lindh, R. Atomic Cholesky Decompositions: A Route to Unbiased Auxiliary Basis Sets for Density Fitting Approximation with Tunable Accuracy and Efficiency. *The Journal of Chemical Physics* **2009**, *130*, 154107.
- (45) Worth, G. Quantics: A general purpose package for Quantum molecular dynamics simulations. *Computer Physics Communications* **2020**, *248*, 107040.

- (46) Mendive-Tapia, D.; Meyer, H.-D. Regularizing the MCTDH equations of motion through an optimal choice on-the-fly (i.e., spawning) of unoccupied single-particle functions. *The Journal of Chemical Physics* **2020**, *153*, 234114.
- (47) Coonjobeeharry, J.; Spinlove, K. E.; Sanz Sanz, C.; Sapunar, M.; Došlić, N.; Worth, G. A. Mixed-quantum-classical or fully-quantized dynamics? A unified code to compare methods. *Philosophical Transactions of the Royal Society A: Mathematical, Physical and Engineering Sciences* **2022**, *380*, 20200386.
- (48) Manthe, U. A time-dependent discrete variable representation for (multiconfiguration) Hartree methods. *The Journal of Chemical Physics* **1996**, *105*, 6989–6994.
- (49) Fiete, G. A.; Heller, E. J. Semiclassical theory of coherence and decoherence. *Physical Review A* **2003**, *68*, 022112.
- (50) Meisner, J.; Vacher, M.; Bearpark, M. J.; Robb, M. A. Geometric Rotation of the Nuclear Gradient at a Conical Intersection: Extension to Complex Rotation of Diabatic States. *Journal of Chemical Theory and Computation* **2015**, *11*, 3115–3122.
- (51) Schwickert, D.; Ruberti, M.; Kolorenč, P.; Usenko, S.; Przystawik, A.; Baev, K.; Baev, I.; Braune, M.; Bocklage, L.; Czwalińska, M. K. et al. Electronic quantum coherence in glycine molecules probed with ultrashort x-ray pulses in real time. *Science Advances* **2022**, *8*, eabn6848.
- (52) Schwickert, D.; Przystawik, A.; Diaman, D.; Kip, D.; Marangos, J. P.; Laarmann, T. Coupled Electron–Nuclear Dynamics Induced and Monitored with Femtosecond Soft X-ray Pulses in the Amino Acid Glycine. *The Journal of Physical Chemistry A* **2024**, *128*, 989–995.
- (53) Lasorne, B.; Robb, M. A.; Worth, G. A. Direct quantum dynamics using variational multi-configuration Gaussian wavepackets. Implementation details and test case. *Physical Chemistry Chemical Physics* **2007**, *9*, 3210.